EVS27
Barcelona, Spain, November 17-20, 2013

On Smoothing HEV/EREV Supervisory Control Action Using an Extended ECMS Approach

Branimir Škugor, Vanja Ranogajec, Joško Deur
University of Zagreb, Faculty of Mechanical Engineering and Naval Architecture, Ivana Lučića 5, Zagreb, Croatia,
Email: branimir.skugor@fsb.hr; vanja.ranogajec@fsb.hr; josko.deur@fsb.hr

Abstract

The paper first describes the previously proposed control strategy for a series-parallel hybrid electric vehicle (HEV) and an Extended Range Electric Vehicle (EREV), which combines a heuristic RB controller with an instantaneous optimisation strategy. The optimisation algorithm is based on the equivalent consumption minimisation strategy (ECMS), which optimises the engine operating point over proper 1D or 2D regions of the engine torque map at every sampling instant. In order to try to minimise the equivalent fuel consumption, the ECMS approach can command frequent changes of engine operating points, thus affecting NVH features of the HEV/EREV power train. The paper proposes and verifies an extended ECMS approach that penalizes for frequent changes of engine operating point, thus being able of reducing the NVH content and in fact improving the fuel economy when applied to a full (forward-looking) power train model.

Keywords: Hybrid electric vehicle, extended range electric vehicle, smoothing, control system, power management, optimisation, NVH

1 Introduction

Production Hybrid Electric Vehicle (HEV) power trains are usually controlled by heuristic/rule-based (RB) control strategies, whose aim is to keep the internal combustion engine within the optimal fuel efficiency operating region [1]. In order to improve the fuel efficiency, a simplified RB approach has been augmented in the authors' previous work [2, 3] by an instantaneous fuel consumption optimisation algorithm based on the equivalent consumption minimisation strategy (ECMS), wherein the battery power flow is reflected to "additional" fuel consumption rate. In order to sustain the battery state-of-charge (*SoC*) within prescribed boundaries, the ECMS is smoothly combined with SoC controller. It has been demonstrated in [2, 3] that the combined RB and ECMS controller can approach the globally optimal solution obtained by using vehicle backward model and dynamic programming optimisation algorithm. However, the RB and ECMS approach can cause rather aggressive engine transients which can affect the vehicle NVH performance, as demonstrated in [4, 5].

In order to improve the NVH performance, the paper proposes an extended ECMS that smoothies the supervisory control action based on penalizing for abrupt transients of commanded engine speed (cf. [4] where a similar basic concept has been applied). The proposed method is applied to the originally considered series-parallel HEV [2, 3], as well as to a more complex extended range electric vehicle (EREV) [6]. It is verified by means of computer simulations, conducted by using both backward and forward vehicle model, and different certified driving cycles (NEDC, HWFET and UDDS).

The paper is organized as follows. Section 2 outlines the HEV/EREV power train models that are used for the purpose of design and simulation verification of the extended control strategy. Section 3 overviews the basic HEV/EREV control strategies. Section 4 proposes the control strategy improvement based on smoothing the engine transients. A comparative simulation analysis of the basic and extended control strategies is presented in Section 5. Concluding remarks are given in Section 6.

2 Power train Modelling

The HEV and EREV transmission modelling is discussed in [2, 7] and [6, 8], respectively. The next two subsections briefly describe the HEV/EREV power train models of both kinematic (backward) and dynamic (forward) type.

2.1 HEV kinematic model

The principal schematic of the considered, quite common series-parallel HEV transmission is shown in Fig. 1a [9]. The transmission consists of two electric machines (M/G1 and M/G2), an internal combustion engine (ICE), a planetary gear as a power split device, and an electrochemical battery. The relationships between the engine, M/G1 and M/G2 torques and speeds are given by the following sets of kinematic equations [2, 3]:

$$\tau_e = (h+1)\tau_{mg1} \ , \tag{1}$$

$$\omega_{mg1} = (h+1)\omega_e - h\omega_{mg2} \ , \tag{2}$$

$$\omega_{cd} = \omega_{mg2} / i_o \ , \tag{3}$$

$$\tau_{cd} = i_o(\tau_{mg2} + h(h+1)^{-1}\tau_e) \ , \tag{4}$$

where the torque $_{(.)}$ and speed $_{(.)}$ variables are defined in Fig. 1a, h is the (fixed) planetary gear ratio, and i_o is the final drive ratio.

The battery is described by a common quasi-static model based on the equivalent battery electrical circuit shown in Fig. 1b, with the open-circuit voltage U_{oc} dependence of state of charge (SoC) plotted in Fig. 2b. The battery internal resistance $R(SoC, i)$ [2] is only made dependent on the battery operating mode (i.e. $R = R_{ic}$ for charging, and $R = R_{idc}$ for discharging). The SoC is only state variable of the battery and overall power train model.

The quasi-stationary (backward) HEV model, described with Eqs. (1)-(4) and the battery SoC state nonlinear equation [10], is used for global numerical optimisation of control variables (off-line optimisation) and also for initial verification of realistic control strategies.

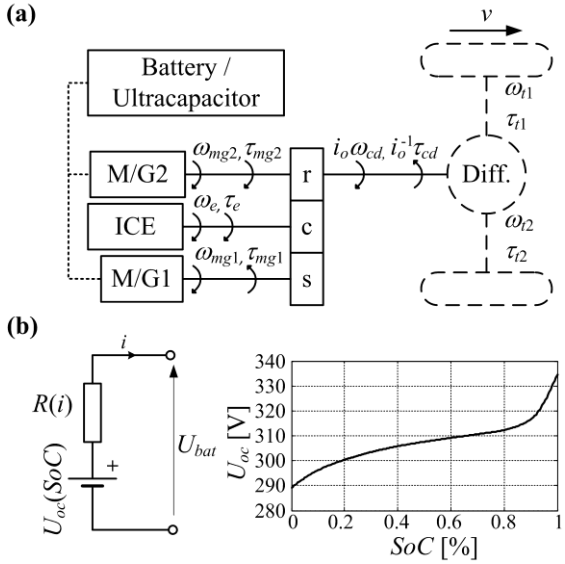

Figure 1: Principal schematic of considered series-parallel hybrid power train (a), and quasi steady-state battery model (b).

2.2 EREV kinematic model

Fig. 2 shows a functional scheme of the considered Extended Range Electric Vehicle (EREV) transmission [6, 11]. Apart the engine, two electric machines, battery and planetary gear, this transmission also includes three clutches (F1, F2, and F3), which are responsible for switching between various operating modes.

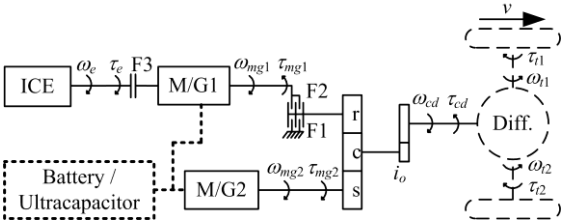

Figure 2: Principal schematic of considered EREV power train.

Table 1: Transmission steady-state equations for different operating modes.

MODE:	ω_{cd}	τ_{cd}
EV, SHEV	$\frac{1}{i_o(h+1)}\omega_{mg2}$	$i_o(h+1)\tau_{mg2}$
SPHEV, TMEV	$\frac{1}{i_o(h+1)}(\omega_{mg2}+h\omega_{mg1})$	$i_o(h+1)\tau_{mg2} =$ $i_o(h+1)h^{-1}(\tau_e-\tau_{mg1})$
MODE:	ω_e	τ_e
EV	0	0
SHEV	ω_{mg1}	τ_{mg1}
SPHEV	ω_{mg1}	$h\tau_{mg2}+\tau_{mg1}$
TMEV	0	0

Depending on the clutch states, the transmission can operate in various operating modes which can be grouped in electric modes that are active during the charge depleting (CD) period, and hybrid electric modes that are used in the charge sustaining (CS) or blended regime. More specifically, there are five characteristic power train operating modes [6, 11] that can be divided into three specific groups. In the first group, characterized by no power split, clutch F1 is locked (F1 = ON), and clutch F2 is open (F2 = OFF). Thus, the ring gear is locked, the planetary gear is reduced to a standard two-port gear, and the M/G2 machine speed is directly proportional to the power train output speed ω_{cd}. Here, clutch F3 is used to switch between electric vehicle mode (EV, F3 = OFF) or series hybrid electric vehicle mode (SHEV, F3 = ON), where the latter also include engine start operation. The second group of operating modes includes the power split feature (F1 = OFF , F2 = ON), where clutch F2 connects the M/G1 machine to the planetary gear, thus combining both electric machines and making their speeds dependent on each other and the output speed ω_{cd}. This results in series-parallel operating mode (SPHEV, F3 = ON), or two machine electric vehicle mode (TMEV, F3 = ON). The third group relates to the power train idle mode, where clutches F1 and F2 are open while F3 can be locked for charging the battery (BC) or starting the engine, or open for fully idle mode.

Table 1 gives equations of the EREV kinematic model, with the notation defined in Fig. 2. This kinematic model is combined with the first-order battery model described in previous subsection, in order to create the backward model used for numerical optimisations and initial verifications and tuning of control strategy.

2.3 HEV/EREV power train dynamics model

Final simulation verifications of the control system are carried out by using a more detailed power train dynamics model (a forward model), which includes driver-submodel, transmission inertia effects, and low-level machine/engine control subsystem.

The driver model [2] is implemented as a proportional-integral (PI) controller which forces an internal vehicle model to follow a prescribed (driving cycle) vehicle velocity time-profile. Its outputs, the transmission output torque and speed demands are used as the forward model inputs.

The HEV transmission dynamics is described by the second-order model [2, 3], which reflects the engine-side and wheel-side lumped inertia effects and the EREV transmission dynamics are described by the fourth-order model [6], which takes into account the inertia effects of engine, M/G1 and M/G2 machine, and vehicle mass referred to wheel shaft. The stick-slip friction of the EREV clutches, is described by a computationally efficient Karnopp model.

These models are used to develop and tune the high-bandwidth low-level PI controller of M/G1 speed, which keeps the engine in its optimal operating point [2, 6] or balance the load in the case of EREV TMEV operating mode. In the case of HEV low-level control strategy, an auxiliary, low-bandwidth proportional (P) controller of engine speed is used, which is aimed at avoiding the engine speed drift due to modelling uncertainties.

3 Basic HEV/EREV Control Strategies

The EREV power train operates in two electric modes (EV and TMEV) and two hybrid modes (SHEV and SPHEV). The HEV control system structure can be utilized in the case of EREV's hybrid modes, and then extended for a maximum-efficiency operation in electric modes.

3.1 HEV/EREV control strategies for SPHEV operating mode

Since the engine, M/G1 machine and M/G2 machine speeds and torques are coupled through the planetary gear kinematics and the driver demand (Eqs. (1)-(4), Table 1), for both HEV and EREV power train structures, it is sufficient to assign the engine speed and engine torque values for the given vehicle velocity and torque demand. The rule-based (RB) HEV/EREV control strategy (see Fig. 3a, [2, 3]) consists of a proportional-like *SoC* controller, engine start/stop logic, and engine operating point calculation. Note that engine start/stop logic contains hysteresis aimed to avoid frequent engine on/off switching.

The engine operating point optimisation is aimed to minimize the equivalent fuel consumption defined by [12, 13]

$$\dot{m}_{eq} = \dot{m}_{fuel} + \dot{m}_{batt}(P_{batt}, \eta_{batt}, A_{ek}), \qquad (5)$$

where the battery power flow is accounted for by the so-called battery equivalent fuel rate $\dot{m}_{batt}$ and combined with the actual engine fuel consumption rate $\dot{m}_{fuel}$, and where P_{batt} is the battery charging/discharging power, η_{batt} is the battery efficiency and A_{ek} is the engine specific fuel

consumption. The driver and battery power demands (P_d and P_{batt}, respectively) are used to determine the engine power demand P_e^*. The 1D-ECMS optimisation minimizes the equivalent fuel consumption (5) over the constant engine power curve $P_e = P_e^*$ (Fig. 4a - red line), thus satisfying the engine power demand and ensuring the *SoC* sustainability (Fig. 3a, [12]). When the *SoC* is around the target value, it is possible to give the ECMS more freedom in order to reduce the fuel consumption [2, 3]. Therefore, a 2D-ECMS is smoothly combined with RB+1D-ECMS through a *SoC* error-dependent weighting function $W(e_{SoC})$ (see Figs. 3b and 4b, [12]). The weighting function deadzone is much narrower for the EREV control strategy since the allowed *SoC* deviation from its target value is lower (± 2%) than in the case of HEV control strategy (±10%; see Fig. 4b).

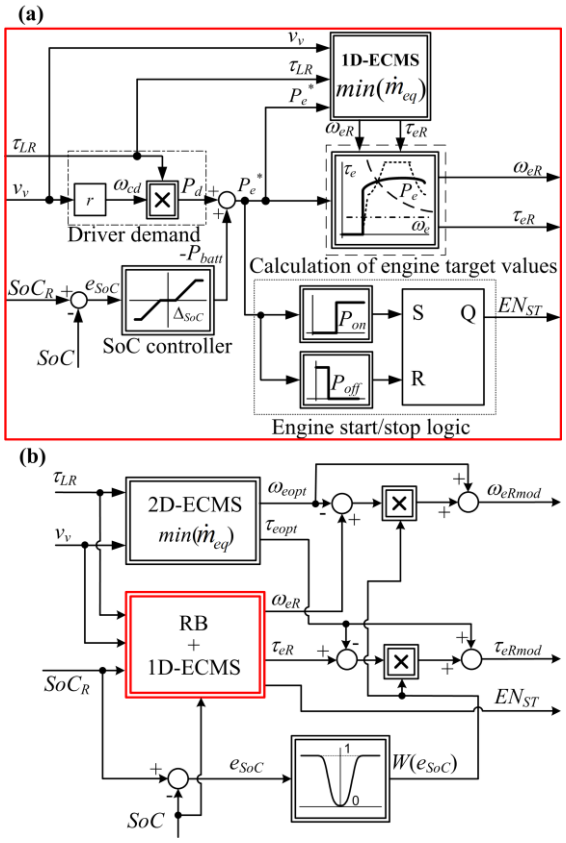

Figure 3: Block diagram of combined RB controller and 1D-ECMS-based optimisation (a), and block diagram of combined RB+1D-ECMS controller extended with 2D-ECMS-based optimisation.

When the *SoC* starts to significantly differ from its target value, the RB+1D-ECMS takes dominance over the 2D-ECMS due to its ability to preserve the *SoC* sustainability while still using ECMS (of 1D type). Fig. 4a shows searching line and searching region for 1D-ECMS and 2D-ECMS control strategies (see [3] for details).

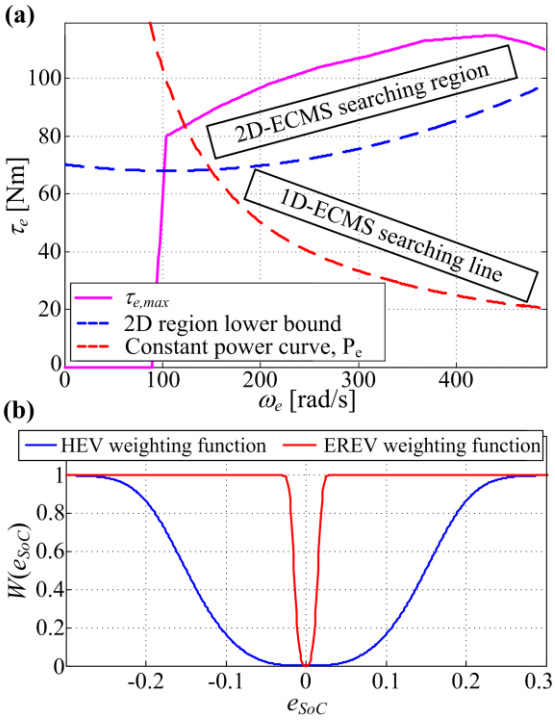

Figure 4: 1D-ECMS searching line and 2D-ECMS searching region (a), and *SoC* control error-dependent weighting function of 2D-ECMS.

3.2 Overall EREV control strategy

Since the EREV power train structure is more complex than the HEV one, its control strategy contains additional rules and laws.

The basic modes of EREV operation are charge depleting (CD) and charge sustaining (CS) modes. The vehicle is driven in the CD mode until the *SoC* reaches some predefined value (30% in this paper), and afterwards it is switched to the CS mode in order to sustain the *SoC*. Consequently, there are two different control strategies: (i) CD mode strategy (electric driving only) and (ii) CS mode strategy (hybrid electric driving). The CD mode includes EV and TMEV operating modes, while the CS mode supports all operating modes (EV, TMEV, SHEV, and SPHEV).

Both, CD and CS strategies consist of two parts: (i) optimal operating mode determination, and (ii) instantaneous optimization of power train operating points for the chosen operating mode and the given driver demand inputs and physical constraints on power train torque and speed variables. Fig. 5 outlines operating modes regions in the output torque vs. vehicle velocity map, whose borders have been obtained by means of offline analyses and dynamic programming optimisation tool [6] (cf.

[11]). In the case of CD regime's EV and TMEV modes, the powertrain operating point is set with the aim to satisfy the driver torque demand, and also to maximize the overall powertrain efficiency (in the case of TMEV mode [6, 7]). In the case of hybrid modes (SPHEV and SHEV), the (engine) operating point is chosen according to the RB+ECMS methodology, as described in the previous subsection.

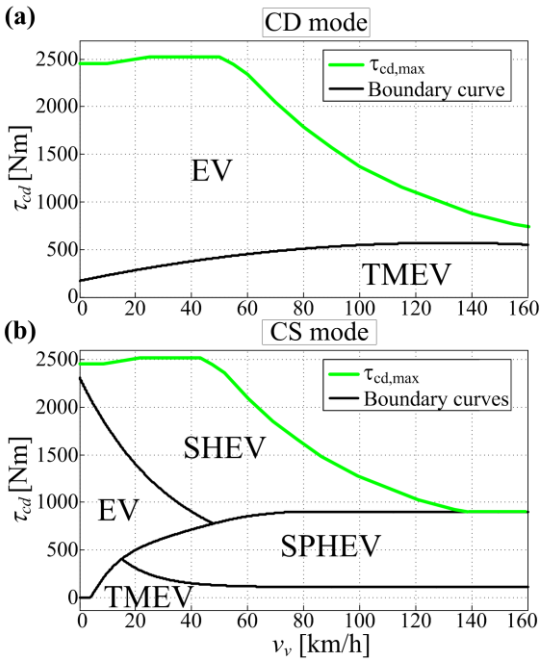

Figure 5: Operating modes and associated regions for the case of CD regime (a), and CS regime (b).

4 Control Strategy Improvement

It is generally necessary to smoothen control variables transients in order to improve the NVH performance, reduce the fuel consumption and slow down vehicle components aging. This can be done by means of simple control variables filtering at the output of (supervisory) controller [5]. However, in an ECMS-based control strategy, it is generally more effective (in terms of reaching optimality in a straightforward way) to extend the ECMS cost function (5) with a term that penalizes for aggressive transients of control variables [4]. Here, the following extended cost function is used:

$$\dot{m}_{eq} = \dot{m}_{fuel} + \dot{m}_{batt}(P_{batt}, \eta_{batt}, A_{ek}) + K(\omega_{eR,i} - \omega_{eR,i-1})^2 / F \quad , \qquad (6)$$

where the additional (third) factor penalizes for the engine speed difference between two consecutive sampling intervals. The factor F is the unit scaling factor, while the weighting factor K is chosen to provide a favourable trade-off between response smoothness and fuel consumption.

5 Simulation Results

Two verification indices are considered in order to asses control strategy improvement benefits. The first index relates to energy consumption, it is denoted below as *f*, and it indicates the percentage of higher fuel consumption compared to the optimal fuel consumption obtained by using the globally optimal dynamic programming-based optimisation algorithm (described in [12] and [14] for HEV and EREV, respectively). The second index represents the standard deviation of engine acceleration, which is considered as an engine/power train NVH indicator.

In order to facilitate calculation of the fuel consumption index *f* for a generally arbitrary final value of the *SoC*, the DP optimisation has been used to find the map of optimal (minimal) fuel consumption for different final *SoC* values. An example of this map, obtained for the EREV and NEDC, is shown in Fig. 6 (black circles), and interpolated by two straight lines. The DP results in Fig. 6 have been obtained by using the backward model, and they are used to assess the fuel consumption for both backward and forward model-based simulations. The relative difference between the actual fuel consumption and the fuel consumption obtained from the DP optimized map in Fig. 6 for the given final *SoC* is defined as the fuel consumption index *f*. Note that interpretation of the index *f* is not quite straightforward in the case of forward model assessment, because the map in Fig. 6 could only be obtained for the backward model. For instance, the fact that negative *f* values may be obtained for the forward model tests (see Table 2 below) does not mean that the fuel consumption is lower than the optimal one, but it is rather a consequence of indirect comparison (based on different models). However, the approach can still be used for comparative (relative) assessment of different control strategies (and parameters) applied to the same forward model.

Simulation and verification have been performed for a number of different values of the weighting factor K in the range from 0 to 1, in order to assess the influence of factor K to the performance indices and to find the optimal one.

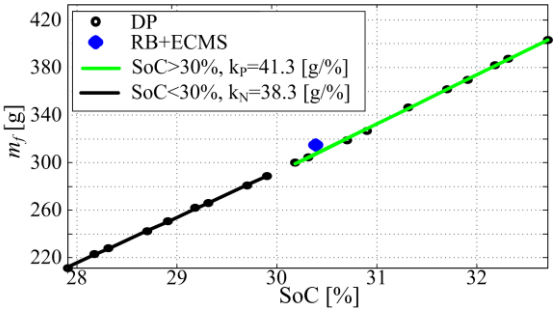

Figure 6: DP optimal results for the case of EREV and NEDC driving cycle.

5.1 HEV simulation results

Fig. 7a shows the engine speed reference time responses for the case of HEV and UDDS driving cycle, and both basic control strategy (K = 0) and improved control strategy with an appropriate weighting factor K > 0. It can be seen from these comparative responses and their details in Fig. 7b that the engine reference value is smoother in the case of using improved control strategy.

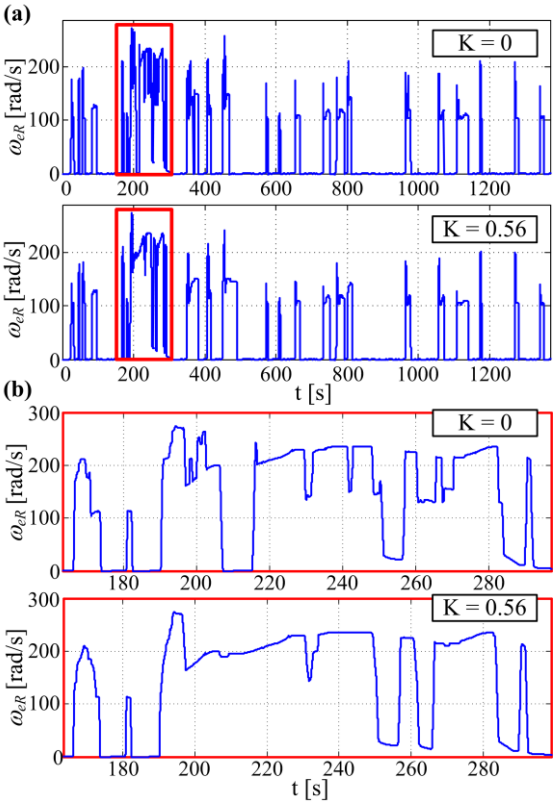

Figure 7: Engine speed reference time responses for HEV case and UDDS driving cycle (a), and their details (b) (red rectangles from (a)).

In order to find an optimal value of the parameter K for all characteristic driving cycles considered (NEDC, HWFET, UDDS), the values of performance indices obtained by using the forward model and every single factor K are summed up for the three driving cycles and shown in a normalized plot (see Fig. 8 for the HEV case). The closest point to the origin should be regarded as the optimal point considering both criteria (the red point in Fig. 8, obtained for K= 0.56).

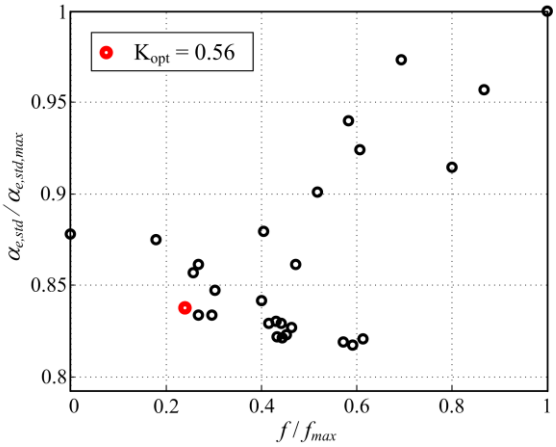

Figure 8: Normalized performance indices plot (HEV, forward model).

Fig. 9 shows values of the fuel consumption index f for different values of the weighting factor K, which have been obtained in the case of HEV and UDDS cycle. As it can be expected, in the case of backward (BWD) model the index f gradually increases (higher fuel consumption) with the growth of factor K, because less emphasis is then given on the fuel consumption minimisation (i.e. ECMS; see Eq. (6)). However, in the case of more realistic forward (FWD) model, the index f is reduced at higher values of the factor K (fuel efficiency improvement).

On the other hand, the engine acceleration standard deviation falls with increase of the parameter K for both backward and forward models (Fig. 10). Table 2 compares the performance indices f and $\alpha_{e,std}$ for the basic and extended HEV control strategy, and the optimal choice of weighting parameter K and the forward vehicle model. The fuel consumption index is calculated as a relative difference between the actual fuel consumption m_f and the DP optimized fuel consumption at the same final SoC, as explained in the previous subsection with Fig. 6. The results in Table 2 indicate that the engine acceleration standard deviation is reduced and the fuel efficiency is somewhat improved for all considered driving cycles when the extended/smoothed control strategy is applied.

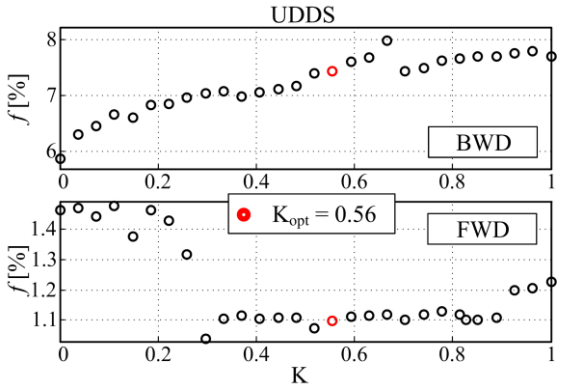

Figure 9: Fuel consumption index vs. weighting factor for backward and forward model (HEV, UDDS).

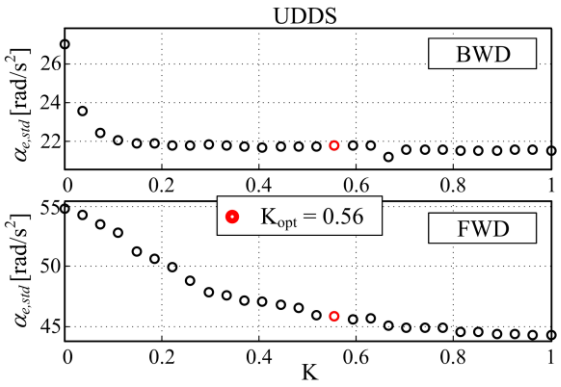

Figure 10: Standard deviation of engine acceleration (HEV).

Table 2: Comparison of performance indices for basic and extended control strategy, for HEV case, forward model, and different driving cycles (K = 0.56).

HEV/NEDC	SoC_{final} [%]	m_{fuel} [g]	f [%]	$\alpha_{e,std}$ [rad/s^2]
RB+ECMS	50.38	263.9	**-1.03**	**24.7**
RB+ECMS ext.	50.70	265.1	**-1.08**	**23.1**
HEV/HWFET	SoC_{final} [%]	m_{fuel} [g]	f [%]	$\alpha_{e,std}$ [rad/s^2]
RB+ECMS	63.13	513.2	**0.20**	**58.7**
RB+ECMS ext.	63.25	513.4	**0.14**	**46.9**
HEV/UDDS	SoC_{final} [%]	m_{fuel} [g]	f [%]	$\alpha_{e,std}$ [rad/s^2]
RB+ECMS	41.53	240.1	**1.46**	**54.8**
RB+ECMS ext.	47.08	264.9	**1.1**	**45.9**

5.2 EREV simulation results

Fig. 11 shows the EREV engine speed reference time responses for several values of the weighting parameter K and the HWFET driving cycle. In the case of basic control strategy (K = 0) the engine speed reference response is characterized by an emphasized chattering effect (high-frequency perturbations; Fig. 11), as opposed to the basic HEV control strategy where this effect was not clearly observed (Fig. 7). The chattering effect is effectively suppressed by applying the extended control strategy (K > 0), as shown in Fig. 11a, and particularly in the corresponding zoomed-in plots in Fig. 11b.

The normalized performance indices plot, shown in Fig. 12, indicates that the optimal value of parameter K equals 0.53 for the EREV.

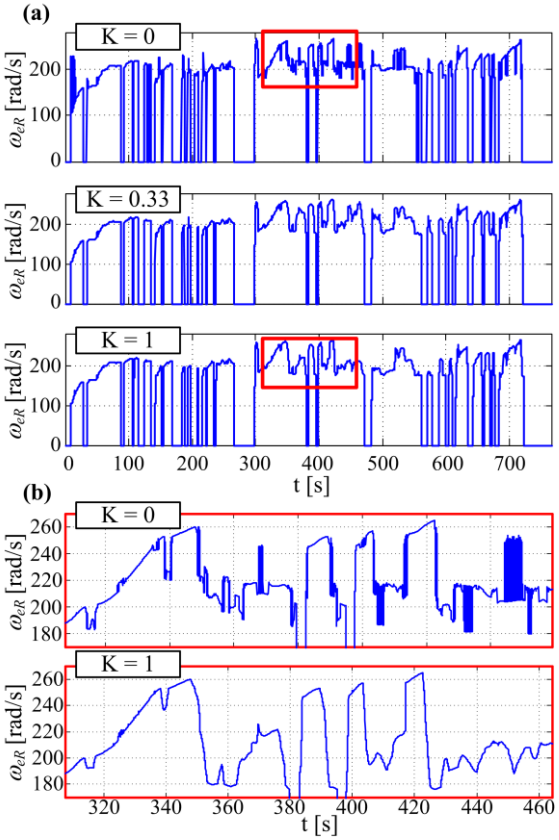

Figure 11: Engine speed reference time responses for EREV case and HWFET driving cycle (a), and their details (b) (red rectangles from (a)).

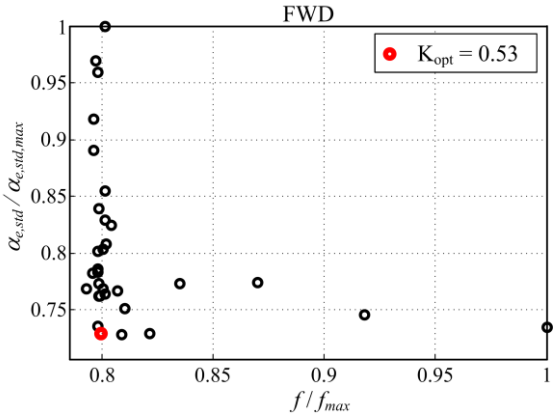

Figure 12: Normalized performance indices plot (EREV, forward model).

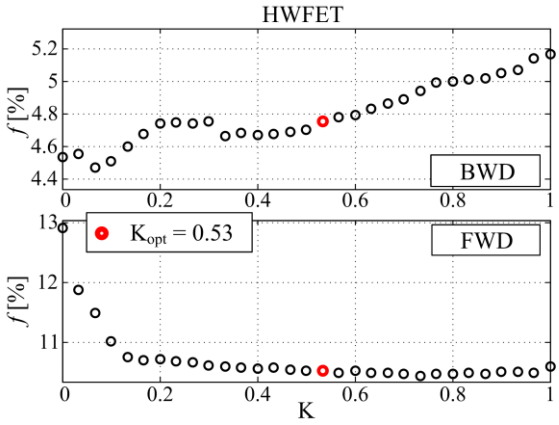

Figure 13: Fuel consumption index vs. weighting factor for backward and forward model (EREV, UDDS).

Figs. 13 and 14 illustrates, that as in the HEV case, the fuel consumption index *f* gradually grows with increase of the weighting factor *K*. Exceptionally, there are a couple of plot points for which *f* slightly reduces with increase of *K*, which may mean that there is a certain possibility for improving the original control strategy (e.g. by optimising some of the control strategy parameters [3, 8]). The results in Fig. 13 (second subplot) and Table 3 show that the fuel efficiency is significantly improved (*f* is significantly reduced) by applying the extended control strategy (with optimal *K*) to the realistic forward vehicle model in the case of NEDC and HWFET driving cycles, while it deteriorates for the UDDS cycle.

As expected, the engine acceleration standard deviation decreases with the growth of parameter *K* in the case of backward model (see the first subplot in Fig. 14). However, in the case of forward model (see the second subplot in Fig.14 and Table 3), the engine acceleration index dependence on the weighting factor differs from the monotonically falling trend. This appears to be because the high-frequency chattering, which is present in the engine speed *reference* signal and filtered out by the extended control strategy (Fig. 11), is largely suppressed in the *real* engine speed signal (used for calculation of the index $\alpha_{e,std}$) by means of the transmission inertia.

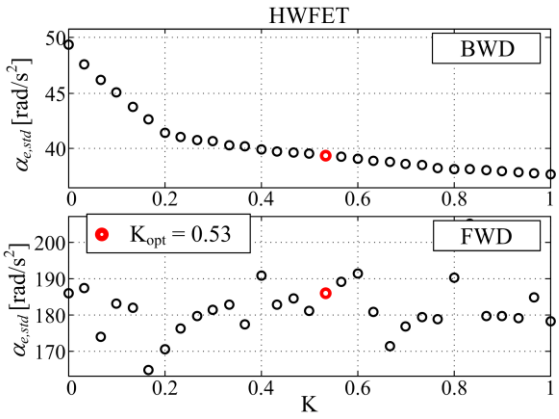

Figure 14: Standard deviation of engine acceleration (EREV).

Table 3: Comparison of performance indices for basic and extended control strategy, for EREV case, forward model, and different driving cycles (*K* = 0.53).

EREV/NEDC	SoC_{final} [%]	m_{fuel} [g]	***f* [%]**	**$\alpha_{e,std}$ [rad/s²]**
RB+ECMS	28.45	261.7	**12.3**	**145.4**
RB+ECMS ext.	28.68	257.8	**6.6**	**117.3**
EREV/HWFET	SoC_{final} [%]	m_{fuel} [g]	***f* [%]**	**$\alpha_{e,std}$ [rad/s²]**
RB+ECMS	32.45	619.4	**12.9**	**186.0**
RB+ECMS ext.	32.59	612.2	**10.5**	**186.0**
EREV/UDDS	SoC_{final} [%]	m_{fuel} [g]	***f* [%]**	**$\alpha_{e,std}$ [rad/s²]**
RB+ECMS	27.92	273.8	**14.5**	**300.4**
RB+ECMS ext.	27.82	269.9	**14.7**	**324.1**

6 Conclusion

The paper has presented a simple extension of the previously proposed RB+ECMS HEV/EREV control strategy with an ECMS term that makes the engine response smoother. The simulation results have demonstrated that the extended strategy effectively suppresses aggressive transients both in the HEV and EREV cases. At the same time, the fuel efficiency is improved in the case of more realistic, dynamic (forward) power train model. The fuel efficiency gain has tuned out to be rather mild in the HEV case, but it can be quite significant in the EREV case. The simulation results have shown that satisfying results can be achieved for all driving cycles using a unique/optimal value of the extended-ECMS weighting factor K for each vehicle. Thus, a complex algorithm of adapting the weighting factor K can be avoided. Because of the above benefits and simple implementation, the extended control strategy is more suitable for real applications than the original control strategy.

Acknowledgments

It is gratefully acknowledged that the presented work has been supported by the Croatian Science Foundation through the project No. 09/128.

References

[1] L. Guzzella, A. Sciaretta, *Vehicle Propulsion Systems*, 2nd ed., Springer Verlag, Berlin, 2007.

[2] B. Škugor, D. Pavković, J. Deur, *A Series-Parallel Hybrid Electric Vehicle Control Strategy Including Instantaneous Optimization of Equivalent Fuel Consumption*, IEEE MSC conference, Dubrovnik, 2012.

[3] B. Škugor, D. Pavković, J. Deur, *A Series-Parallel HEV Control Strategy Combining SoC Control and Instantaneous Optimisation of Equivalent Fuel Consumption*, EEVC Brussels, Belgium, 19-22, 2012.

[4] J. Arata, M. Leamy, K. Cunefare, *Power-Split HEV Control Strategy Development with Refined Engine Transients*, SAE Paper 2012-01-0629, 2012.

[5] Y. Kim, T. K. Lee, Z. Filipi, *Frequency Domain Power Distribution Strategy for Series Hybrid Electric Vehicles*, SAE Paper 2012-01-1003, 2012.

[6] B. Skugor, J. Deur, *Instantaneous Optimization-based Energy Management Control Strategy for Extended Range Electric Vehicle*, SAE Technical Paper 2013-01-1460, 2013.

[7] M. Cipek, J. Deur, J. Petrić, *Bond Graph Modeling and Power Flow Analysis of Series-Parallel HEV Transmissions*, International Journal of Power Trains, Vol. 1, No. 4, pp. 396 – 419, 2012.

[8] J. Deur, M. Cipek, B. Skugor, and J. Petric, *Modeling and Low-level Control of Range Extended Electric Vehicle Dynamics*, International Conference on Powertrain Modeling and Control (PMC 2012), West Yorkshire, UK, 2012.

[9] J. M. Miller, *Comparative Assessment of Hybrid Vehicle Power Split Transmission*, 4th VI Winter Workshop Series, PPT presentation, January 12, 2005.

[10] J. Liu, H. Peng, *Modeling and Control of a Power-Split Hybrid Vehicle*, IEEE Transactions on Control Systems Technology, Vol. 16, No. 6, November 2008.

[11] M. A. Miller, A. G. Holmes, B. M. Conlon and P. J. Savagian, *The GM "Voltec" 4ET50 Multi-Mode Electric Transaxle*, SAE Paper 2011-01-0887, 2011.

[12] B. Škugor, J. Deur, M. Cipek, and D. Pavković, *Design of a Power-split HEV Control System Containing Rule-based Controller and Equivalent Consumption Minimisation Strategy*, submitted to Part D: Journal of Automobile Engineering, 2013.

[13] G. Paganelli, Y. Guezennec, G. Rizzoni, *Optimizing Control Strategy for Hybrid Fuel Cell Vehicle*, SAE paper No. 2002-01-0102, SAE International, 2002.

[14] M. Cipek, M. Čorić, B. Škugor, J. Kasać and J. Deur, *Dynamic Programming-based Optimization of Control Variables of Extended Range Electric Vehicle*, SAE Technical Paper 2013-01-1481, 2013.

Authors

Branimir Škugor is a Research Assistant at the University of Zagreb, working on the project entitled "ICT-aided integration of Electric Vehicles into the Energy Systems with a high share of Renewable Energy Sources". His research interests include hybrid electric vehicles control strategies, optimisation algorithms, and probability analyses.

Vanja Ranogajec is an M.S. student at the Faculty of Mechanical Engineering and Naval Architecture of the University of Zagreb. His B.Sc. Thesis included a portion of the work presented in this paper.

Joško Deur is a Full Professor at the University of Zagreb, where he teaches courses in electrical machines and servodrives, digital control systems, and automotive mechatronics. In 2000, he was a guest researcher at the Ford Research Laboratory, Dearborn, MI. Professor Deur has led numerous projects including those supported by Ford Motor Company and Jaguar Cars Ltd. His main research interests include modeling and control of automotive systems and control of electrical servo-drives.